Molecular Modeling, Design, and Synthesis of Less Lipophilic Derivatives of 3-(4-Tetradecyloxybenzyl)-4*H*-1,2,4-oxadiazol-5-one (PMS1062) Specific for Group II Enzyme[‡]

Stéphanie Plocki,[a] Darina Aoun,[a] Azali Ahamada-Himidi,[a] Fernanda Tavarès-Camarinha,[a] Chang-Zhi Dong,[a] France Massicot,[a,b] Jack Huet,[a] Sylvie Adolphe-Pierre,[c] François Chau,[a] Jean-Jacques Godfroid,[a] Nohad Gresh,[d] Jean Edouard Ombetta,[a] and Françoise Heymans*[a]

Keywords: Molecular modeling / $sPLA_2$ / Inflammation / Oxadiazolone

3-(4-Tetradecyloxybenzyl)-4*H*-1,2,4-oxadiazol-5-one (PMS1062 or **I**) can probably act as a PLA_2-II inhibitor on the acute inflammation model, but its highly lipophilic character could prevent it from being biodistributed effectively. In this work, based on a molecular modeling study, we have proposed a model that may provide compounds retaining both anti-PLA_2 activity and specificity while becoming active per os. Moreover, molecular dynamics and energy minimization enabled us to characterize the lowest-energy complexes of each derivative. Energy balances taking account of the conformational energy changes of both partners, along with the drug–protein interaction, were performed, and were further completed by single-point computations of the contributions of solvation/desolvation to the binding. The ordering of the resulting energy balances was found to be fully consistent with the experimentally ascertained ordering of affinities inferred from the IC_{50} values. The essential role of an indole group partaking in cation–π and hydrophobic interactions, together with the Ca^{II}-chelating oxadiazolone ring, was highlighted for the best binding compound.

Introduction

Phospholipases A_2 (PLA_2s) constitute a superfamily of intracellular and secreted enzymes catalyzing the hydrolysis of glycerophospholipids at the *sn*-2-position, resulting in the release of fatty acids and lysophospholipids.[1] PLA_2s are involved in pathophysiological processes by producing arachidonic acid from membrane phospholipids, a phenomenon giving rise to the biosynthesis of various types of pro-inflammatory eicosanoids and lipids. These include prostaglandins, leukotrienes, thromboxanes, metabolites of oxygenated arachidonic acid, and the Platelet Activating Factor(PAF). The involvement of PLA_2s in cellular proliferation, apoptosis, and in some cancers has also been suggested.[2]

The most widely studied PLA_2s to date are a low molecular weight (14 kDa) secreted PLA_2 ($sPLA_2$) and a high molecular weight (85 kDa) intracellular PLA_2 ($cPLA_2$).[3] Numerous other PLA_2 activities have recently been reported, implying that PLA_2s are much more diverse than previously anticipated.[3] Secreted PLA_2s were initially divided into three main groups (I, II, III) according to similarities found in their primary sequences.[4,5] With the recent cloning of several new $sPLA_2$s, this family of proteins has now expanded to encompass ten different groups.[6–12] Among these, secreted nonpancreatic PLA_2 ($snpPLA_2$) was identified as a 14 kDa group II enzyme, calcium-dependent at millimolar concentrations, which preferentially hydrolyzes phospholipids in negatively charged form.

A pivotal role of group II PLA_2 in inflammatory processes has been demonstrated.[13–18] Regulation of these enzymes could therefore be essential against inflammation, which has prompted a search for specific inhibitors of group II PLA_2s vs. group I (pancreatic PLA_2s). The first synthesis of nanomolar inhibitors was reported in 1996 by Lilly.[19–21] Our own group is actively engaged in the search of inhibitors preferentially targeting nonpancreatic over pancreatic PLA_2s.

[‡] Inhibition of Secretory Phospholipases A_2, 3. Part 2: C. Z. Dong et al., *Bioorg. Med. Chem.* **2005,** *13,* 1989–2007.

[a] Unité de Pharmacochimie Moléculaire et Systèmes Membranaires (EA2381), Laboratoire de Pharmacochimie Moléculaire, Université Paris 7 – Denis Diderot, case 7066,
2 Place Jussieu, 75251 Paris Cédex 05, France
E-mail: heymans@ccr.jussieu.fr
[b] Laboratoire de Toxicologie, UFR des Sciences Pharmaceutiques et Biologiques, Université Paris 5 – René Descartes,
4 Avenue de l'Observatoire, 75270 Paris Cédex, France
[c] Département de Chimie, Université des Antilles et de la Guyanne,
B. P. 771, 97173 Pointe-à-Pitre Cédex, France
[d] Laboratoire de Pharmacochimie Moléculaire et Cellulaire, CNRS FRE 2718, UFR Biomédicale, Université René Descartes (PARISV),
45 rue des Saints-Pères, 75006 Paris, France

This has led us to the discovery of our lead compound PMS1062 (**I**), which possesses a micromolar IC_{50} value (Figure 1).

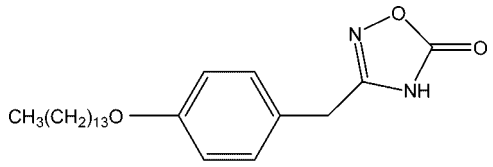

I

Figure 1. Chemical structure of PMS1062 (**I**).

Its structure presents three features: a) a negative moiety binding Ca^{II} at the active site (we found that the oxadiazolone ring, as previously described in other antiinflammatory drugs,[22] was able to play this role), b) a phenoxy group targeting the hydrophobic residues Phe5, Leu2, and Val30, observed in proximity to the Ca^{II} binding site in the X-ray crystal structure,[23] and c) a paraffinic chain of 14 carbon atoms, introduction of which had previously been shown by us to be optimal for PLA_2 inhibition.[24] Furthermore, the presence of this paraffinic chain has analogy in natural PLA_2 substrates. In vitro tests demonstrated this compound to have both anti-group II PLA_2 activity at a micromolar level and selectivity for nonpancreatic over pancreatic PLA_2. In vivo studies, however, revealed it to be active by intraperitoneal administration but inactive per os, probably due to its high lipophilicity, with a partition coefficient ($\log P$) of 7.1 units. Reduction of $\log P$ therefore appears necessary to provide an orally active drug. While a straightforward process consisted of a progressive reduction of the aliphatic chain length of PMS1062, the consequence was a drastic decrease in the activity or even its complete disappearance.[24] The design of compounds retaining both anti-PLA_2 activity and specificity while becoming active per os constitutes the objective of this study. To this end we resorted to a combined approach using molecular modeling, chemical synthesis, and enzymatic inhibition assays. Consideration of the crystal structure of PLA_2 in its complex with (4*S*)-4-[(1-oxo-7-phenylheptyl)amino]-5-[(phenylmethyl)phenylthio]pentanoic acid (OAP) shows the presence of electron-deficient (Arg, Lys), aromatic (His), and aliphatic (Ile, Val) residues as potential ligand recognition sites in the vicinity of the Ca^{II} binding site.[23] We therefore designed and subsequently synthesized and tested a series of derivatives of PMS1062 based on this model, each containing an indole ring connected to the phenoxy moiety through a paraffinic chain of variable length (n = 3, 5–8, 10), to evaluate the optimal distance for the best activity. The indolyl moiety was chosen for its propensity to partake in cation–π,[25] as well as π–π and van der Waals interactions.

In future studies, the nature of this linker and that of the terminal aromatic group will both be modified in an effort to enhance the inhibitory potency further and to decrease the lipophilicity.

Chemistry

N-(ω-Bromoalkyl)indoles **1a**–**f** were prepared according to Dehaen et al.[26] (see Scheme 1), by monosubstitution of dibromoalkanes with indole. These bromo derivatives were then condensed with *p*-hydroxyphenylacetonitrile in the form of its sodium salt to form intermediates **2a**–**f**. The nitrile functions were converted into amidoximes **3a**–**f** by treatment with hydroxylamine, and addition of phenyl chloroformate and subsequent heating gave the substituted oxadiazolones **II**–**VII** (Figure 2).

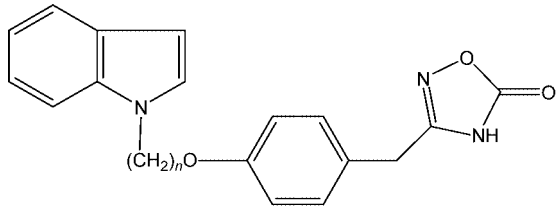

n = 3 (**II**); n = 5 (**III**); n = 6 (**IV**); n = 7 (**V**); n = 8 (**VI**); n = 10 (**VII**)

Figure 2. Chemical structures of **II** to **VII**.

Results and Discussion

The lowest-energy structure obtained by Molecular Dynamics (MD) for the complex of PMS1062 with PLA_2 (Figure 3) was used as a starting point for the design of the indole-containing analogues. In these analogues, the paraffinic tail of PMS1062 was replaced by *N*-indolylalkyl chains bearing variable numbers of methylene groups (n = 3, 5, 6, 7, 8, 10) (Figure 2).

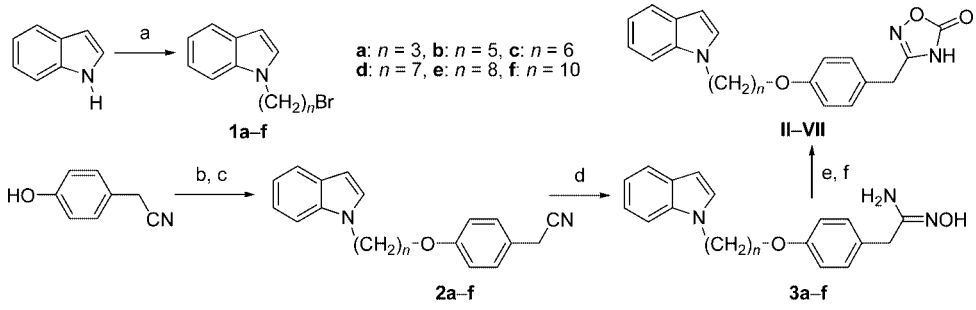

Scheme 1. Reagents and conditions: a) CH_3CN, K_2CO_3, $Br(CH_2)_nBr$, reflux, 5 d. b) NaOH, EtOH, 0 °C, 1 h. c) **1a**–**f**, DMF, room temp., 3 d. (d) NH_2OH HCl, K_2CO_3, EtOH, reflux, 18 h. e) PhOCOCl, Et_3N, CH_2Cl_2, 0 °C, 1 h. (f) $PhCH_3$, reflux, 5 h.

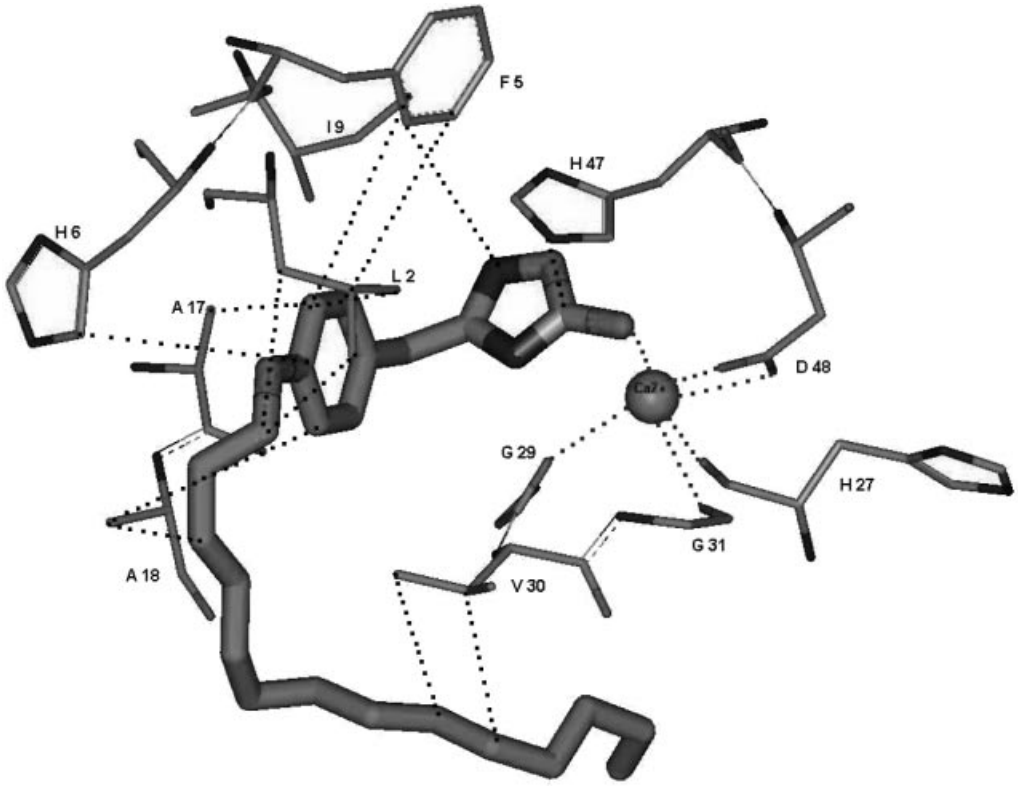

Figure 3. Representation of the most important interactions occurring between PMS1062 and the binding site of PLA_2 as derived from molecular dynamics with Accelrys software and the cff91 forcefield.

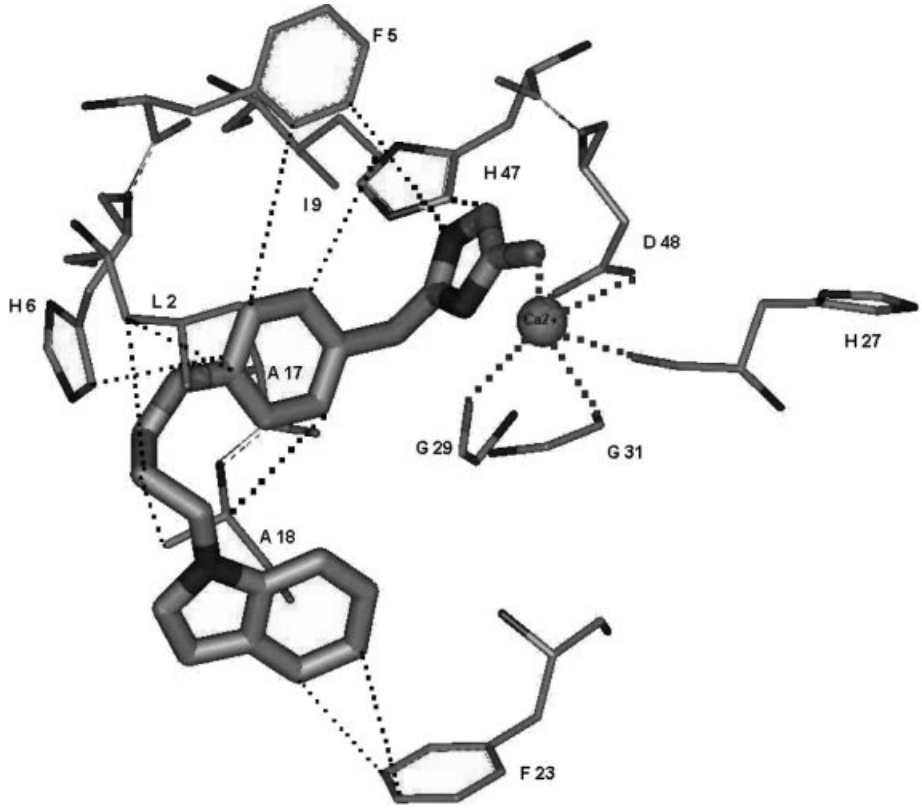

Figure 4. Representation of the most important interactions occurring between **II** and the binding site of PLA_2 as derived from molecular dynamics with Accelrys software and the cff91 forcefield.

Figure 3 shows the contribution of the paraffinic tail, involving interactions only with the side chains of the aliphatic residues Ala18 and Val30. On the other hand, though, there is also proximity of additional aromatic and aliphatic residues (namely, Phe5, His6, Leu2) to the phenoxy ring, together with that of the cationic residue Arg7. Therefore, in an attempt to gain further stabilization by targeting these residues, we replaced the paraffinic side chain by an indolylalkyl chain. The choice of indolyl moiety was motivated by its propensity to partake in cation–π interactions,[25] as well as π–π and van der Waals interactions.

The structures of the most stable complexes obtained from the MD approach are presented in Figures 4, 5, 6, 7, 8, and 9, for compounds **II**–**VII**, respectively.

The energy balances resulting from the modeling, together with the experimentally measured inhibitory potencies, are listed in Tables 1, 2, and 3.

Table 1 shows in vacuo energy balances obtained with $\varepsilon = 4 \times r$. E_{int} represents the value of the inhibitor–protein interaction energy, δE_{lig} and δE_{prot} denote the variations of conformational energies of the inhibitor and the protein, respectively, upon passing from the uncomplexed to the complexed state, and δE is the sum: $E_{int} + \delta E_{lig} + \delta E_{prot}$.

Let us denote the values of the energies of the protein and of the ligand after energy minimization in the absence of complexation by E_{0prot} and E_{0lig}, respectively.

We denote the energies of separated protein and ligand, as extracted from the lowest-energy MD frame, by E_{prot} and

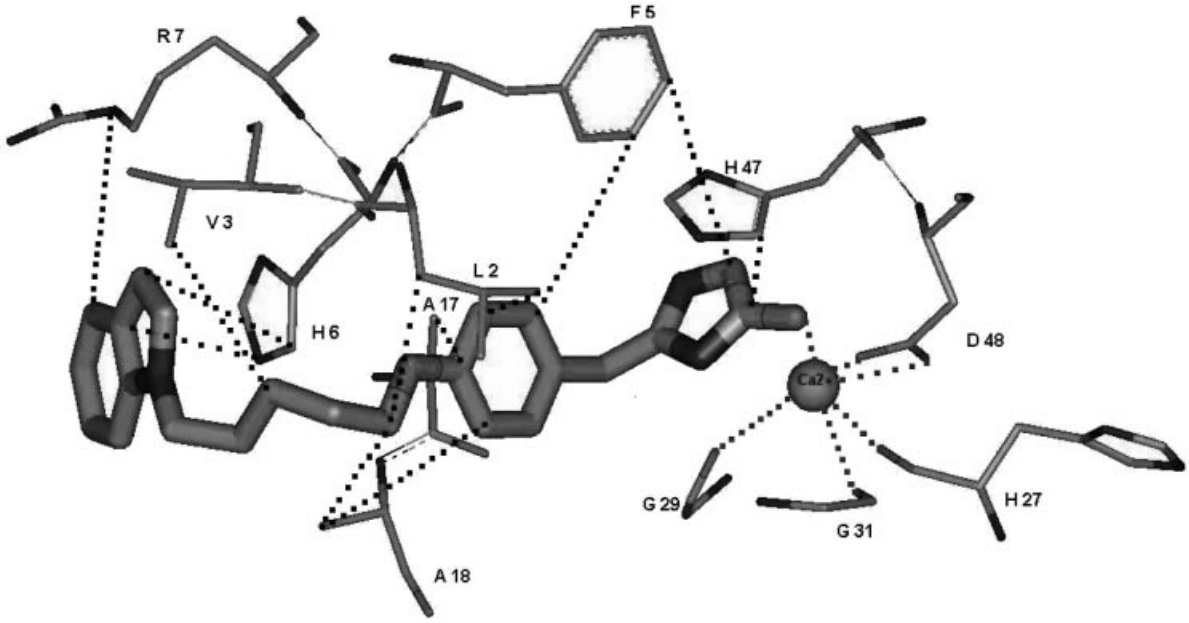

Figure 5. Representation of the most important interactions occurring between **III** and the binding site of PLA_2 as derived from molecular dynamics with Accelrys software and the cff91 forcefield.

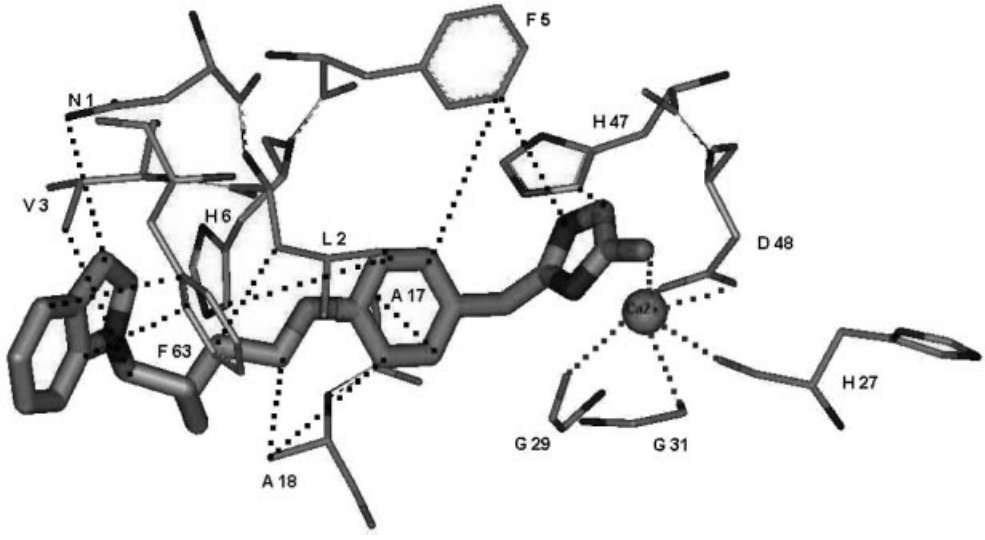

Figure 6. Representation of the most important interactions occurring between **IV** and the binding site of PLA_2 as derived from molecular dynamics with Accelrys software and the cff91 forcefield.

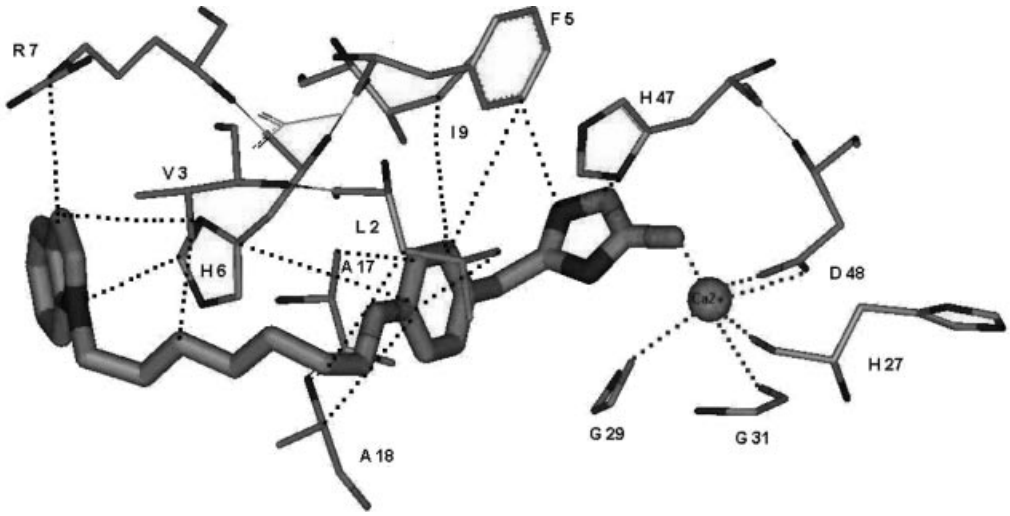

Figure 7. Representation of the most important interactions occurring between **V** and the binding site of PLA_2 as derived from molecular dynamics with Accelrys software and the cff91 forcefield.

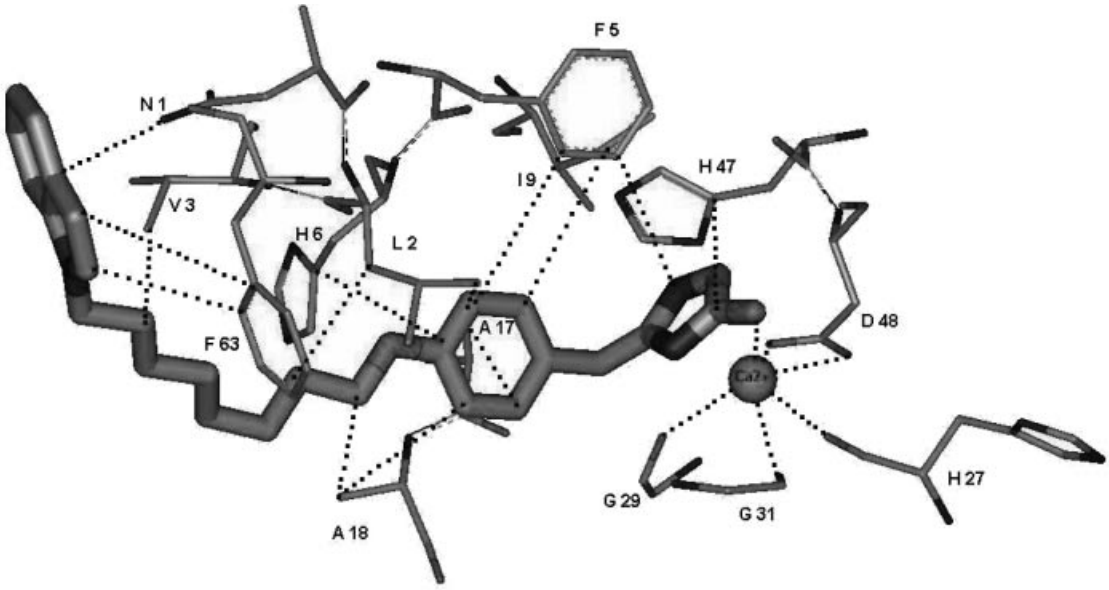

Figure 8. Representation of the most important interactions occurring between **VI** and the binding site of PLA_2 as derived from molecular dynamics with Accelrys software and the cff91 forcefield.

E_{lig}, respectively, and the total energy of the corresponding complex by E_{tot}. Then:

$\delta E_{prot} = E_{0prot} - E_{prot}$

$\delta E_{lig} = E_{0lig} - E_{lig}$

$E_{int} = E_{tot} - E_{prot} - E_{lig}$

Table 2 gives related energy balances after single-point Poisson–Boltzmann calculations of continuum solvation energies on the same structures as in Table 1. The values of E_{int}, δE_{lig}, δE_{prot}, and δE_1 were now recomputed for the corresponding structures with $\varepsilon = 4$.

Table 3 reports the same energy balances, now carried out on the best structures obtained from MD with $\varepsilon = 4$ instead of $\varepsilon = 4 \times r$.

In Tables 2 and 3 (with the effect of continuum solvation):

$\delta E_1 = E_{int} + \delta E_{prot} + \delta E_{lig}$

In these two tables, $E_{solvprot}$ and $E_{solvlig}$ denote the continuum solvation energies of the isolated protein and the ligand, respectively, after in vacuo energy minimization in the absence of complexation, whilst $E_{solvtot}$ denotes the continuum energy of the complex. Then:

$\delta E_{solv} = E_{solvtot} - E_{solvlig} - E_{solvprot}$

and finally:

$\delta E_2 = \delta E_1 + \delta E_{solv}$

In the indolylalkyl derivative series, compound **III** (n = 5) shows the strongest inhibitory potency. Its IC_{50} of 5.0 μM is equivalent to that of the lead compound **I** (PMS1062) (IC_{50} = 4 μM), but its partition coefficient ($\log P$) of 3.8 units has decreased by 3.2 in relation to **I** ($\log P$ = 7.1). This

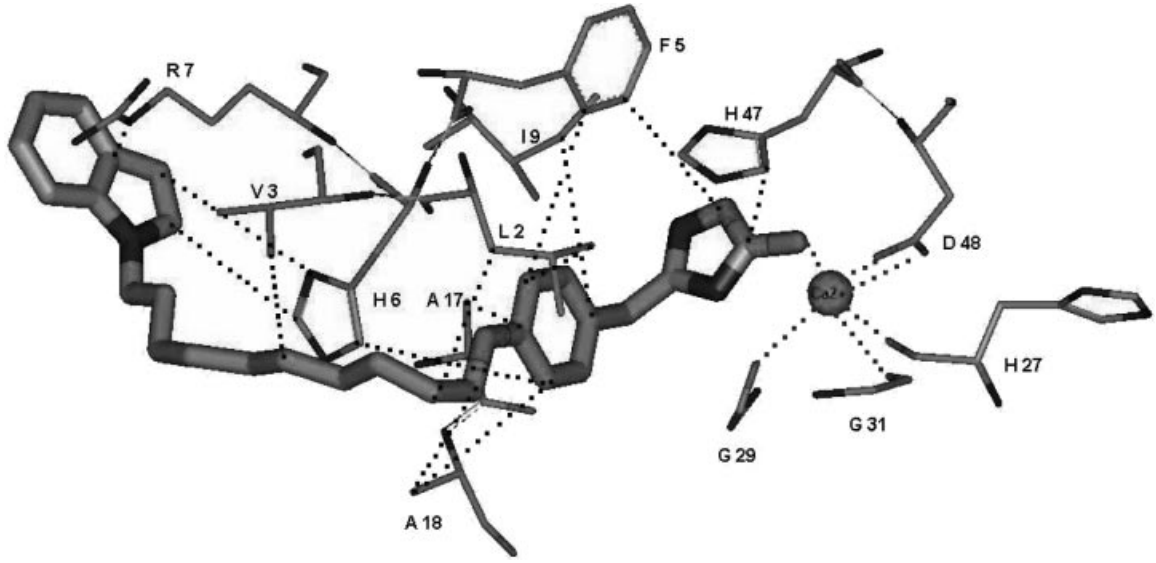

Figure 9. Representation of the most important interactions occurring between **VII** and the binding site of PLA_2 as derived from molecular dynamics with Accelrys software and the cff91 forcefield.

Table 1. Energy balances ($\varepsilon = 4 \times r$) resulting from molecular modeling and the experimentally determined inhibitory potencies.

Cmpd.	n	E_{int}	δE_{prot}	δE_{lig}	δE	IC_{50} (μM) hGIIA	IC_{50} (μM) pGIB
II	3	–71.3	4.3	8.7	–58.3	70 ± 0.1	>100
III	5	–60.3	0.5	6.7	–53.1	5 ± 0.7	>100
IV	6	–60.7	0.5	6.7	–53.5	15 ± 0.1	>100
V	7	–59.3	1.3	7.9	–50.1	14 ± 0.2	>100
VI	8	–60.8	0.4	4.9	–55.5	11 ± 1.2	>100
VII	10	–63.5	1.3	6.0	–56.2	8 ± 1.8	>100
I		–68.0	0.4	6.7	–60.9	4 ± 0.4	>100

corresponds to an increase by a factor of a thousand in its solubility in aqueous phase. Compound **II** (n = 3) has the smallest inhibitory potency, 14 times smaller than that of **III**. Increasing n to more than five first results in a decrease in the inhibitory potency (**IV**: n = 6; **V**: n = 7), followed by real increases for n = 8 and 10, which is not surprising for compounds reaching the same level of lipophilicity as **I**. Therefore, the combination of both IC_{50} and partition coefficient clearly point to derivative **III** (n = 5) as the most promising in the series.

All compounds are anchored to the active site by a bidentate interaction of oxadiazolone with Ca^{II}, occurring through the extracyclic oxygen atom of the carbonyl group and the nitrogen atom close to it. In all compounds, the phenoxy ring has stacking/van der Waals interactions with Phe5, Leu2, and Ala18. For compounds **II**–**VII**, the extent and nature of interactions of the indolyl group depends upon the linker length. For n = 3 (Figure 4) this ring only partakes in a stacking interaction with Phe23. For n = 5,

Table 2. Energy balances (ε = 4) after single-point Poisson–Boltzmann calculations of continuum solvation energies, together with the experimentally determined inhibitory potencies.

Cmpd.	n	E_{int}	δE_{prot}	δE_{lig}	δE_1	$E_{solvtot}$	$E_{solvlig}$	$E_{solvprot}$	δE_{solv}	δE_2	IC_{50} (μM)
II	3	–122.1	8.8	8.7	–104.6	–338.2	–21.8	–385.1	68.7	–35.9	70 ± 0.1
III	5	–129.5	5.5	8.1	–115.9	–344.3	–22.5	–385.1	63.3	–52.6	5 ± 0.7
IV	6	–121.0	9.9	8.1	–103.0	–346.7	–22.3	–385.1	60.7	–42.3	15 ± 0.1
V	7	–128.2	6.3	12.7	–109.2	–354.2	–22.4	–385.1	62.3	–46.9	14 ± 0.2
VI	8	–130.1	6.4	12.9	–110.8	–354.2	–22.7	–385.1	62.6	–48.5	11 ± 1.2
VII	10	–132.8	7.8	10.6	–114.4	–343.7	–23.9	–385.1	65.3	–49.1	8 ± 1.8
I		–130.9	9.9	9.1	–111.9	–349.0	–23.6	–385.1	59.7	–52.2	4 ± 0.4

Table 3. Energy balances, now carried out on the best structures obtained from MD (Table 1) with ε = 4 instead of $\varepsilon = 4 \times r$, together with the experimentally determined inhibitory potencies.

Cmpd.	n	E_{int}	δE_{prot}	δE_{lig}	δE_1	$E_{solvtot}$	$E_{solvlig}$	$E_{solvprot}$	δE_{solv}	δE_2	IC_{50} (μM)
II	3	–115.6	2.9	6.5	–106.8	–367.1	–24.3	–409.0	66.2	–40.6	70 ± 0.1
III	5	–121.6	2.3	7.5	–111.7	–373.3	–25.3	–409.0	61.0	–50.7	5 ± 0.7
IV	6	–113.2	2.4	7.7	–102.9	–374.0	–25.5	–409.0	60.5	–42.4	15 ± 0.1
V	7	–119.2	2.6	5.9	–113.1	–363.1	–23.2	–409.0	69.1	–44.0	14 ± 0.2
VI	8	–122.6	0.2	5.7	–107.2	–373.0	–24.3	–409.0	60.3	–46.9	11 ± 1.2
VII	10	–127.4	9.7	9.6	–117.6	–365.8	–25.9	–409.0	69.1	–48.5	8 ± 1.8
I		–128.4	0.2	8.9	–116.6	–366.9	–23.1	–409.0	65.2	–51.4	4 ± 0.4

(Figure 5), the indolyl group partakes in simultaneous interactions with His6 (parallel stacking), Arg7, and Val3. For $n = 6$ (Figure 6), it stacks in a T-shape orientation over Phe63, while the NH_2 group of Asn1 stacks above its five-membered ring. For $n = 7$ (Figure 7), the indole ring has a T-shaped stacking with His6 and enters into van der Waals interactions with Arg7. For $n = 8$ (Figure 8) it interacts through the electron-rich cloud of its five-membered ring with the NH_2 group of Asn1 and is also engaged in a stacking interaction with the benzene ring of Phe63, although the interplanar separation (4.4 Å) is longer than standard. For $n = 10$ (Figure 9), it makes a cation–π complex with Arg7 and participates in a van der Waals interaction with His6.

The energy balances given in Table 1 with $\varepsilon = 4 \times r$ do not show any correlation between δE and the experimentally measured IC_{50} values. Thus, even though compound **I** has the greatest absolute value of δE, consistent with it having the lowest IC_{50} value, compound **III**, with a pentamethylene spacer, ranking second best in terms of experimental inhibitory potencies in this series, has a δE value smaller in magnitude than the longer chain homologues with $n = 8$ (**VI**) and 10(**VII**) methylene groups. This indicates the inadequacies of performing energy balances with an oversimplified representation of solvation effects. In contrast, the energy balances in Table 2 show a striking agreement with the ordering of biological data. Thus, the absolute values of δE decrease in the sequence:

III ($n = 5$) ≥ **I** (PMS1062) > **VII** ($n = 10$) > **VI** ($n = 8$) > **V** ($n = 7$) > **IV** ($n = 6$) > **II** ($n = 3$)

while the IC_{50} values increase in the following sequence, indicative of decreasing affinities:

I (PMS1062) ≤ **III** ($n = 5$) < **VII** ($n = 10$) < **VI** ($n = 8$) < **V** ($n = 7$) < **IV** ($n = 6$) < **II** ($n = 3$)

The only inversion in these two sequences concerns compounds **III** and **I**, but it bears on extremely small differences both in δE (0.4 kcal mol^{-1}) and in IC_{50} (1 μM). The obtaining of such an agreement is satisfactory in view of the approximations involved in this approach, which uses only single-point computations of Poisson–Boltzmann solvation energies for the most stable minima of the MD procedure. Such agreement may mean that compounds **II**–**VII**, differing only in the lengths of their paraffinic connectors, can be differentiated by the extent of overlap of their indole rings with their target PLA_2 sites (Val3, His6, Arg7, Phe23, Phe63...), as well as by the variable amount of solvent exposure of such residues in the complexes. The need to include the solvation effects is illustrated by the corresponding sequence of δE_1 values, as found before accounting for δE_{solv}:

III ($n = 5$) > **VII** ($n = 10$) > **I** (PMS1062) > **VI** ($n = 8$) > **V** ($n = 7$) > **II** ($n = 3$) > **IV** ($n = 6$)

in which **I** is ranked third rather than first while the relative affinities of **II** and **IV** are inverted. Nevertheless, among the designed compounds even prior to accounting for solvation effects, **III** ($n = 5$) is the one endowed with the largest magnitude of δE_1.

The energy balances given in Table 3, in which single-point computations of the solvation energies are carried out on the selected MD frames with $\varepsilon = 4 \times r$, give a ranking of δE values fully consistent with the corresponding ones from Table 2 and actually identical with the sequence of experimentally determined inhibitory potencies:

I (PMS1062) ≥ **III** ($n = 5$) > **VII** ($n = 10$) > **VI** ($n = 8$) > **V** ($n = 7$) > **IV** ($n = 6$) > **II** ($n = 3$)

The need to include solvation energies is here again shown by the inconsistency in the corresponding ordering of δE_1 values in their absence:

VII ($n = 10$) > **I** (PMS1062) > **V** ($n = 7$) > **III** ($n = 5$) > **VI** ($n = 8$) > **II** ($n = 3$) > **IV** ($n = 6$)

Conclusion and Perspectives

We have previously reported[27] the design and synthesis of an oxadiazolone derivative, PMS1062, possessing a 4 μM inhibitory potency for group II PLA_2s. Its log *P* value of 7.1, however, prevents its per os bioavailability. This has prompted us to design novel derivatives that should be equivalent to PMS1062 in terms of binding affinity but with reduced log *P* values. This was done in this study by replacing the long paraffinic chain of PMS1062 by an indolylalkyl component of variable length (3–10 methylene moieties for the alkyl group). Variable-length connector derivatives ($n = 3$, 5–8, and 10 methylene groups) based on the results from molecular modeling were synthesized. Their in vitro inhibitory potencies were experimentally measured as described previously.

In this series, compound **III**, with $n = 5$ methylene groups, was both computed and measured to have the highest PLA_2 binding affinities. The essential contribution of its indole ring in stabilization, through cation–π and hydrophobic interactions, was highlighted by the modeling studies. Compound **III**, furthermore, has a log *P* value of only 3.7 units, below the threshold value of 5, above which bioavailability[28] is hampered. As such, compound **III** appears to be the most interesting for future developments, and so we are currently evaluating the impact of incorporating an additional Ca^{II}-chelating group into **III**, which should enhance both PLA_2 binding affinity and solubility. The results will be reported in due course.

To have reached the same ranking of affinities as determined experimentally after accounting for solvation is certainly encouraging, in view of the fact that the ΔG_{solv} values obtained by the Poisson–Boltzmann procedure were derived only from single-point computations on the best frames from MD. This may signify that the relative affinities of the designed compounds, differing only in the lengths of their paraffinic connectors, are modulated predominantly by the overlap of their indole rings with their target PLA_2 sites (Val30, His6, Arg7, Phe23, Phe63...), and that the use of $\varepsilon = 4$ or $\varepsilon = 4 \times r$ in the course of MD could partly mimic the structural effects of solvation on these aspects. We intend to attempt to refine the energy balances in more general series of derivatives by resorting to the polarizable molecular me-

chanics procedure SIBFA,[29] recently used in conjunction with the Langlet–Claverie methodology for continuum solvation[30] to investigate the binding of inhibitors to metalloenzymes.[31,32] There is ongoing progress in the incorporation of continuum solvation models in the course of energy minimization or molecular dynamics,[33,34] and we plan to use these in future studies.

Experimental Section

Molecular Modeling: The molecular dynamics computations were carried out with the DISCOVER (Accelrys) software.[35] We used the 2 Å resolution X-ray crystal structure of hsnp-PLA_2 complexed with micromolar inhibitor OAP[23] (PDB access code 1kvo). The computations were carried out on the 70 N-terminal residues of PLA_2, and included the Ca^{II} ion of the active site. Restriction to these residues was supported by the X-ray structure, which showed all drug–protein interactions to take place exclusively in the N-terminal part. The ligands were constructed with the Builder module of the Accelrys package,[35] with use of the cff91 forcefield. To derive the atomic charges on the oxadiazolone fragment in its anionic state, a Mulliken population analysis was performed following an ab initio Hartree–Fock computation with the 6-311G** basis set and the Gaussian 98 package.[36] Energy minimization and molecular dynamics were performed in the absence of explicit water molecules. Two different protocols were carried out for each complex. The first was with a distance-proportional dielectric screening ($4 \times r$), and the second was with a fixed ε of 4. Throughout the simulations, the protein backbone was held frozen, while the side-chains, the Ca^{II} cation, and the inhibitor were relaxed. Manual docking, followed by a preliminary round of energy minimization, was performed by use of our computer graphic facilities prior to molecular dynamics. The latter used the same protocol as described.[37] After 5000 fs initialization steps at 300 K, 100 steps of molecular dynamic calculations were performed. Each was done at 300 K during 5000 steps of 1 fs. The resulting structure was subjected to conjugate-gradient energy minimization and stored. All 100 structures are characterized by an ionic bond between Ca^{II} and the C–O oxygen atom of the oxadiazolone ring. The search for the best conformation of the uncomplexed protein and inhibitors was carried out by the same molecular dynamics protocol. Solvation energies of the selected minima were computed using the Poisson–Boltzmann procedure with the Delphi software.[38] The solute and solvent dielectric constants were 4 and 80, respectively.

Chemistry. General Methods: All materials were obtained from commercial suppliers and were used without further purification. Thin-layer chromatography was performed on TLC plastic sheets coated with silica gel ($60F_{254}$, layer thickness 0.2 mm, Merck). Column chromatography purification was carried out on silica gel 60 (70–230 mesh ASTM, Merck). All melting points were determined with a digital melting point apparatus (Electrothermal) and are uncorrected. IR and ^1H NMR spectra confirmed the structures of all compounds. IR spectra were obtained in paraffin oil with an ATI Mattson Genesis Series FTIR spectrometer, and ^1H NMR spectra were recorded in $CDCl_3$ with a Bruker AC 200 spectrometer with hexamethyldisiloxane (HMDS) as an internal standard. Chemical shifts are given in ppm and peak multiplicities are designated as follows: s, singlet; d, doublet; t, triplet; quint, quintuplet; m, multiplet. Elemental analyses were obtained from the "Service Régional de Microanalyse" (Université Paris 6 – Pierre et Marie Curie), Paris, France, and were within ±0.4% of theoretical values.

***N*-(3-Bromopropyl)indole (1a):** A stirred mixture of 1,3-dibromopropane (58.95 g, 0.25 mol), K_2CO_3 (11.8 g, 85.5 mmol), and indole (10 g, 85.5 mmol) was heated to reflux in acetonitrile (200 mL) for 5 d. The solvent was removed under vacuum, and the oily residue was dissolved in EtOAc (150 mL), washed with water (2×75 mL), and dried with magnesium sulfate. After filtration, the organic phase was concentrated in vacuo, and the crude product was purified by silica gel column chromatography, first with petroleum ether and then with 5% ether in petroleum ether as eluents to afford **1a** (12 g, 40%) as a colorless oil: ^1H NMR (200 MHz, $CDCl_3$): δ = 2.16 (m, 2 H, CH_2), 3.12 (t, J = 6.09 Hz, 2 H, CH_2Br), 4.15 (t, J = 6.3 Hz, 2 H, CH_2N), 6.41 (d, J = 3.15 Hz, 1 H, H_{ar}), 6.94–7.15 (m, 3 H, H_{ar}), 7.24 (d, J = 8.30, 1 H, H_{ar}), 7.53 (d, J = 7.63, 1 H, H_{ar}) ppm. ^{13}C NMR (50 MHz, $CDCl_3$): δ = 30.46, 32.60, 43.83, 101.42, 109.19, 119.42, 121.00, 121.56, 127.91, 128.62, 135.72 ppm.

***N*-(5-Bromopentyl)indole (1b):** This compound was prepared in a similar manner in 52% yield (yellow oil). ^1H NMR (200 MHz, $CDCl_3$): δ = 0.81 (m, 2 H, CH_2), 1.46 (m, 4 H, CH_2), 3.23 (t, J = 6.68 Hz, 2 H, CH_2Br), 3.95 (t, J = 7 Hz, 2 H, CH_2N), 6.39 (d, J = 3.00 Hz, 1 H, H_{ar}), 6.93–7.23 (m, 4 H, H_{ar}), 7.52 (d, 1 H, H_{ar}) ppm. ^{13}C NMR (50 MHz, $CDCl_3$): δ = 25.42, 29.24, 33.29, 45.94, 100.91, 108.16, 119.12, 120.84, 121.26, 127.59, 128.47, 135.72 ppm. IR (neat): $\tilde{\nu}$ = 3052, 2937, 2863 cm^{-1}.

***N*-(6-Bromohexyl)indole (1c):** 46% (green oil). ^1H NMR (200 MHz, $CDCl_3$): δ = 1.36 (m, 4 H, CH_2), 1.70 (m, 4 H, CH_2), 3.28 (t, J = 6.50 Hz, 2 H, CH_2Br), 4.03 (t, J = 6.90 Hz, 2 H, CH_2N), 6.39 (m, 1 H, H_{ar}), 6.95–7.16 (m, 3 H, H_{ar}), 7.26 (d, J = 8.53, 1 H, H_{ar}), 7.55 (ddd, J_1 = 8.18, J_2 = 0.82, J_3 = 1.27, 1 H, H_{ar}) ppm. ^{13}C NMR (50 MHz, $CDCl_3$): δ = 26.09, 27.69, 30.01, 32.50, 33.67, 46.13, 100.91, 109.26, 119.15, 120.91, 121.30, 127.69, 128.52, 135.86 ppm. IR (neat): $\tilde{\nu}$ = 3052, 2933, 2857 cm^{-1}.

***N*-(7-Bromoheptyl)indole (1d):** 72% (green oil). ^1H NMR (200 MHz, $CDCl_3$): δ = 1.30 (m, 6 H, CH_2), 1.70 (m, 4 H, CH_2), 3.22 (t, J = 6.75 Hz, 2 H, CH_2Br), 4.02 (t, J = 7.05 Hz, 2 H, CH_2N), 6.39 (dd, J_1 = 3.12, J_2 = 0.70 Hz, 1 H, H_{ar}), 6.97–7.16 (m, 3 H, H_{ar}), 7.26 (d, J = 8.18 Hz, 1 H, H_{ar}) 7.55 (d, J = 7.06, 1 H, H_{ar}) ppm. ^{13}C NMR (50 MHz, $CDCl_3$): δ = 26.75, 27.90, 28.11, 30.06, 32.56, 33.79, 46.24, 100.83, 109.27, 119.10, 120.87, 121.25, 127.68, 128.50, 135.85 ppm. IR (neat): $\tilde{\nu}$ = 3053, 2931, 2855 cm^{-1}.

***N*-(8-Bromooctyl)indole (1e):** 71% (orange oil). ^1H NMR (200 MHz, $CDCl_3$): δ = 1.31 (m, 8 H, CH_2), 1.82 (m, 4 H, CH_2), 3.38 (t, J = 6.80 Hz, 2 H, CH_2Br), 4.10 (t, J = 7.03 Hz, 2 H, CH_2N), 6.50 (d, J = 2.87 Hz, 1 H, H_{ar}), 7.08–7.28 (m, 3 H, H_{ar}) 7.36 (d, J = 8.00 Hz, 1 H, H_{ar}), 7.67 (d, J = 7.66 Hz, 1 H, H_{ar}) ppm. ^{13}C NMR (50 MHz, $CDCl_3$): δ = 26.75, 27.91, 28.47, 28.92, 30.06, 32.59, 33.85, 46.21, 100.75, 109.25, 119.04, 120.82, 121.18, 127.65, 128.47, 135.82 ppm. IR (neat): $\tilde{\nu}$ = 3052, 2930, 2854 cm^{-1}.

***N*-(10-Bromodecyl)indole (1f):** 90% (yellow oil). ^1H NMR (200 MHz, $CDCl_3$): δ = 1.22 (m, 12 H, CH_2), 1.74 (m, 4 H, CH_2), 3.30 (t, J = 6.80 Hz, 2 H, CH_2Br), 4.07 (t, J = 7.02 Hz, 2 H, CH_2N), 6.47 (d, J = 2.90 Hz, 1 H, H_{ar}), 6.99–7.31 (m, 4 H, H_{ar}), 7.63 (d, J = 7.49 Hz, 1 H, H_{ar}) ppm. ^{13}C NMR (50 MHz, $CDCl_3$): δ = 26.67, 27.86, 28.44, 28.94, 29.10, 29.94, 32.55, 33.74, 45.99, 100.59, 109.11, 118.87, 120.64, 121.00, 127.44, 128.36, 135.70 ppm. IR (neat): $\tilde{\nu}$ = 3052, 2928, 2853 cm^{-1}.

{4-[3-(Indol-1-yl)propoxy]phenyl}acetonitrile (2a): A solution of NaOH (0.2 g, 5 mmol) in EtOH (10 mL) was added dropwise at 0 °C to a solution of 4-hydroxybenzyl cyanide (0.70 g, 5.26 mmol) in EtOH (10 mL), and the mixture was stirred at 0 °C for 1 h. The solvent was removed in vacuo, and the residue, dissolved in DMF (15 mL), was added dropwise to a solution of **1a** (1.00 g, 4.02 mmol) in DMF (15 mL). The reaction mixture was stirred at

room temperature for 12 h. The solvent was then removed, and the product was taken up in AcOEt, washed with water, dried with $MgSO_4$, and filtered, and the solvents were evaporated. The residue was purified on a silica gel column with 30% dichloromethane in petroleum ether to yield **2a** (1.1 g, 91%) as a pale yellow oil: ^{1}H NMR (200 MHz, $CDCl_3$): δ = 2.17 (m, 2 H, CH_2), 3.54 (s, 2 H, CH_2CN), 3.74 (t, J = 5.74 Hz, 2 H, CH_2O), 4.26 (t, J = 6.56 Hz, 2 H, CH_2N), 6.40 (d, J = 3.10 Hz, 1 H, H_{ind}), 6.76 (d, J = 8.40 Hz, 2 H, Ph-H), 6.96–7.06 (m, 3 H, H_{ind}), 7.11 (d, J = 8.40, 2 H, Ph-H), 7.27 (d, J = 8.02 Hz, 1 H, H_{ind}), 7.55 (d, J = 7.68 Hz, 1 H, H_{ind}) ppm. ^{13}C NMR (50 MHz, $CDCl_3$): δ = 22.67, 29.63, 42.55, 64.26, 101.22, 109.20, 114.96, 118.12, 119.28, 120.92, 121.46, 121.97, 127.99, 128.54, 129.05, 135.80, 158.31 ppm. IR (neat): $\tilde{\nu}$ = 2249 (CN), 1611 (C=C) cm^{-1}.

{4-[5-(Indol-1-yl)pentoxy]phenyl}acetonitrile (2b): 75% (green oil): ^{1}H NMR (200 MHz, $CDCl_3$): δ = 1.37 (m, 2 H, CH_2), 2.17 (m, 4 H, CH_2), 3.52 (s, 2 H, CH_2CN), 3.79 (t, J = 6.35 Hz, 2 H, CH_2O), 4.26 (t, J = 6.94 Hz, 2 H, CH_2N), 6.40–7.57 (m, 10 H, H_{ar}) ppm. ^{13}C NMR (50 MHz, $CDCl_3$): δ = 22.61, 23.44, 28.70, 29.86, 46.10, 67.58, 100.87, 109.25, 114.93, 115.86, 118.18, 119.12, 120.86, 121.26, 121.57, 127.71, 128.48, 128.95, 129.06, 135.80, 158.58 ppm. IR (neat): $\tilde{\nu}$ = 2249 (CN), 1612 (C=C) cm^{-1}.

{4-[6-(Indol-1-yl)hexoxy]phenyl}acetonitrile (2c): 85% (yellow oil): ^{1}H NMR (200 MHz, $CDCl_3$): δ = 1.35 (m, 4 H, CH_2), 1.65 (m, 4 H, CH_2), 3.53 (s, 2 H, CH_2CN), 3.80 (t, J = 6.30 Hz, 2 H, CH_2O), 4.02 (t, J = 7.01 Hz, 2 H, CH_2N), 6.40–7.57 (m, 10 H, H_{ar}) ppm. ^{13}C NMR (50 MHz, $CDCl_3$): δ = 22.77, 25.71, 26.71, 29.02, 30.16, 46.25, 67.80, 100.92, 109.35, 115.04, 118.27, 119.19, 120.96, 121.34, 121.63, 127.78, 128.58, 129.05, 135.93, 158.77 ppm. IR (neat): $\tilde{\nu}$ = 2249 (CN), 1612 (C=C) cm^{-1}.

{4-[7-(Indol-1-yl)heptoxy]phenyl}acetonitrile (2d): 61% (orange oil). ^{1}H NMR (200 MHz, $CDCl_3$): δ = 1.30 (m, 6 H, CH_2), 1.69 (m, 4 H, CH_2), 3.55 (s, 2 H, CH_2CN), 3.80 (t, J = 6.38 Hz, 2 H, CH_2O), 4.02 (t, J = 7.02 Hz, 2 H, CH_2N), 6.40–7.57 (m, 10 H, H_{ar}) ppm. ^{13}C NMR (50 MHz, $CDCl_3$): δ = 22.69, 25.81, 26.84, 28.90, 28.98, 30.08, 46.26, 67.84, 100.79, 109.27, 114.96, 118.18, 119.08, 120.85, 121.22, 121.50, 127.69, 128.46, 128.96, 135.85, 158.74 ppm. IR (neat): $\tilde{\nu}$ = 2248 (CN), 1612 (C=C) cm^{-1}.

{4-[8-(Indol-1-yl)octoxy]phenyl}acetonitrile (2e): 70% (yellow oil): ^{1}H NMR (200 MHz, $CDCl_3$): δ = 1.25 (m, 8 H, CH_2), 1.69 (m, 4 H, CH_2), 3.54 (s, 2 H, CH_2CN), 3.81 (t, J = 6.41 Hz, 2 H, CH_2O), 4.01 (t, J = 7.03 Hz, 2 H, CH_2N), 6.40–7.57 (m, 10 H, H_{ar}) ppm. ^{13}C NMR (50 MHz, $CDCl_3$): δ = 22.73, 25.86, 26.86, 29.06, 29.10, 30.15, 46.31, 67.95, 100.78, 109.31, 115.00, 118.21, 119.09, 120.87, 121.23, 121.50, 127.72, 128.50, 128.98, 135.88, 158.80 ppm. IR (neat): $\tilde{\nu}$ = 2249 (CN), 1612 (C=C) cm^{-1}.

{4-[10-(Indol-1-yl)decoxy]phenyl}acetonitrile (2f): 70% (yellow oil): ^{1}H NMR (200 MHz, $CDCl_3$): δ = 1.21 (m, 12 H, CH_2), 1.68 (m, 4 H, CH_2), 3.55 (s, 2 H, CH_2CN), 3.84 (t, J = 6.50 Hz, 2 H, CH_2O), 4.02 (t, J = 7.10 Hz, 2 H, CH_2N), 6.40–7.57 (m, 10 H, H_{ar}) ppm. ^{13}C NMR (50 MHz, $CDCl_3$): δ = 22.72, 25.90, 26.93, 29.11, 29.15, 29.22, 29.33, 30.17, 46.31, 68.02, 100.75, 109.31, 115.00, 118.20, 119.07, 120.86, 121.21, 121.47, 127.72, 128.50, 128.97, 135.87, 158.83 ppm. IR (neat): $\tilde{\nu}$ = 2249 (CN), 1611 (C=C) cm^{-1}.

***N*-Hydroxy-2-{4-[5-(indol-1-yl)pentoxy]phenyl}acetamidine (3b):** A mixture of the nitrile **2b** (2.50 g, 7.86 mmol), hydroxylamine hydrochloride (3.00 g, 43.2 mmol), and K_2CO_3 (6.00 g, 43.5 mmol) in absolute EtOH (100 mL) was heated at reflux for 18 h. The salts were filtered and washed with hot absolute EtOH (2×30 mL), and the filtrate was concentrated under reduced pressure. The residue was chromatographed on a silica gel column with CH_2Cl_2 as eluent to yield the amidoxime **3b** (2.4 g, 85%) as a viscous yellow product. ^{1}H NMR (200 MHz, $CDCl_3$): δ = 1.43 (t, 2 H, CH_2), 1.71 (m, J = 7.1 Hz, 4 H, CH_2), 3.31 (s, 2 H, CH_2–C=N), 3.81 (t, J = 6.28 Hz, 2 H, CH_2O), 4.00 (t, J = 6.9 Hz, 2 H, CH_2N), 4.39 (s, 2 H, NH_2), 6.39 (d, J = 3.12 Hz, 1 H, H_{ind}), 6.74 (d, J = 8.60, 2 H, Ph-H), 6.98–7.16 (m, 3 H, H_{ind}), 7.07 (d, J = 8.60 Hz, 2 H, Ph-H), 7.28 (d, J = 7.44 Hz, 1 H, H_{ind}), 7.55 (d, J = 7.13 Hz, 1 H, H_{ind}) ppm. ^{13}C NMR (50 MHz, $CDCl_3$): δ = 23.55, 28.83, 29.95, 36.71, 46.20, 67.55, 100.92, 109.27, 114.72, 119.16, 120.91, 121.31, 127.67, 127.73, 128.52, 129.87, 135.85, 153.28, 158.09 ppm. IR (neat): $\tilde{\nu}$ = 3496, 3391 (NH_2), 3180 (OH), 1663 (C=N) cm^{-1}.

***N*-Hydroxy-2-{4-[3-(indol-1-yl)propoxy]phenyl}acetamidine (3a):** 64% (yellow oil). ^{1}H NMR (200 MHz, $CDCl_3$): δ = 2.17 (quintt, J = 6.30 Hz, 2 H, CH_2), 3.32 (s, 2 H, CH_2CN), 3.75 (t, J = 5.70 Hz, 2 H, CH_2O), 4.27 (t, J = 6.58 Hz, 2 H, CH_2N), 4.41 (s, 2 H, NH_2), 6.40–7.56 (m, 10 H, H_{ar}) ppm. ^{13}C NMR (50 MHz, $CDCl_3$): δ = 29.71, 36.71, 42.65, 64.24, 101.20, 109.25, 114.75, 119.29, 120.93, 121.46, 128.01, 128.08, 128.58, 129.94, 135.83, 153.22, 157.80 ppm. IR (neat): $\tilde{\nu}$ = 3493, 3435 (NH_2), 3207 (OH), 1661 (C=N) cm^{-1}.

***N*-Hydroxy-2-{4-[6-(indol-1-yl)hexoxy]phenyl}acetamidine (3c):** 80% (yellow oil). ^{1}H NMR (200 MHz, $CDCl_3$): δ = 1.34 (m, 4 H, CH_2), 1.71 (m, 4 H, CH_2), 3.31 (s, 2 H, CH_2CN), 3.80 (t, J = 6.26 Hz, 2 H, CH_2O), 4.04 (t, J = 7.00 Hz, 2 H, CH_2N), 4.41 (s, 2 H, NH_2), 6.40–7.56 (m, 10 H, H_{ar}) ppm. ^{13}C NMR (50 MHz, $CDCl_3$): δ = 25.66, 26.66, 29.02, 30.10, 36.65, 46.18, 67.64, 100.84, 109.27, 114.71, 119.14, 120.885, 121.26, 127.50, 127.70, 128.49, 129.85, 135.85, 153.25, 158.16 ppm. IR (neat): $\tilde{\nu}$ = 3493, 3381 (NH_2), 3223 (OH), 1661 (C=N) cm^{-1}.

***N*-Hydroxy-2-{4-[7-(indol-1-yl)heptoxy]phenyl}acetamidine (3d):** 84% (yellow oil). ^{1}H NMR (200 MHz, $CDCl_3$): δ = 1.31 (m, 6 H, CH_2), 1.70 (m, 4 H, CH_2), 3.32 (s, 2 H, CH_2CN), 3.80 (t, J = 6.39 Hz, 2 H, CH_2O), 4.04 (t, J = 7.04 Hz, 2 H, CH_2N), 4.39 (s, 2 H, NH_2), 6.40–7.56 (m, 10 H, H_{ar}) ppm. ^{13}C NMR (50 MHz, $CDCl_3$): δ = 25.90, 26.90, 28.95, 29.10, 30.14, 36.72, 46.33, 67.82, 100.83, 109.31, 114.77, 119.13, 120.91, 121.27, 127.45, 127.73, 128.52, 129.87, 135.89, 153.36, 158.28 ppm. IR (neat): $\tilde{\nu}$ = 3495, 3386 (NH_2), 3199 (OH), 1663 (C=N) cm^{-1}.

***N*-Hydroxy-2-{4-[8-(indol-1-yl)butoxy]phenyl}acetamidine (3e):** 62%, (yellow oil). ^{1}H NMR (200 MHz, $CDCl_3$): δ = 1.26 (m, 8 H, CH_{2al}), 1.65 (m, 4 H, CH_{2al}), 3.31 (s, 2 H, CH_2CN), 3.82 (t, J = 6.33 Hz, 2 H, CH_2O), 4.02 (t, J = 7.01 Hz, 2 H, CH_2N), 4.39 (s, 2 H, NH_2), 6.40–7.56 (m, 10 H, H_{ar}) ppm. ^{13}C NMR (50 MHz, $CDCl_3$): δ = 25.89, 26.87, 29.13, 30.16, 36.72, 46.32, 67.87, 100.79, 109.31, 114.74, 119.10, 120.88, 121.23, 127.53, 127.73, 128.51, 129.86, 135.88, 153.30, 158.26 ppm. IR (neat): $\tilde{\nu}$ = 3495, 3387 (NH_2), 3208 (OH), 1663 (C=N) cm^{-1}.

***N*-Hydroxy-2-{4-[10-(indol-1-yl)decoxy]phenyl}acetamidine (3f):** 89%, (yellow oil). ^{1}H NMR (200 MHz, $CDCl_3$): δ = 1.21 (m, 12 H, CH_{2al}), 1.70 (m, 4 H, CH_{2al}), 3.32 (s, 2 H, CH_2CN), 3.84 (t, J = 6.37 Hz, 2 H, CH_2O), 4.03 (t, J = 7.01 Hz, 2 H, CH_2N), 4.39 (s, 2 H, NH_2), 6.40–7.56 (m, 10 H, H_{ar}) ppm. ^{13}C NMR (50 MHz, $CDCl_3$): δ = 25.95, 26.95, 29.19, 29.37, 30.19, 36.72, 46.35, 67.97, 100.76, 109.32, 114.76, 119.08, 120.87, 121.22, 127.42, 127.74, 128.51, 129.85, 135.89, 153.35, 158.32 ppm. IR (neat): $\tilde{\nu}$ = 3487, 3346 (NH_2), 3234 (OH), 1663 (C=N) cm^{-1}.

3-{4-[3-(Indol-1-yl)propoxy]benzyl}-4*H*-1,2,4-oxadiazol-5-one (II): Phenyl chloroformate (0.38 mL, 2.97 mmol) was added dropwise to a solution of the amide oxime **3a** (0.80 g, 2.47 mmol) and Et_3N (0.52 mL, 3.71 mmol) in CH_2Cl_2 (50 mL), cooled in an ice bath. After stirring at 0 °C for 1 h, the solution was washed with water (2×25 mL), dried ($MgSO_4$), and concentrated in vacuo. The resi-

due was taken up with toluene, and heated to reflux for 4 h. The solvent was removed with a rotary evaporator, and the crude product was chromatographed on a silica gel column with CH_2Cl_2 as eluent to yield the oxadiazolone **II** (0.5 g, 59%) as a beige solid; m.p. 134.4 °C. ^{1}H NMR (200 MHz, [D$_6$]DMSO): δ = 2.18 (m, 2 H, CH_2), 3.79 (s, 2 H, CH_2CN), 3.85 (t, J = 5.98 Hz, 2 H, CH_2O), 4.33 (t, J = 6.65 Hz, 2 H, CH_2N), 6.43 (d, J = 2.87 Hz, 2 H, H_{ind}), 6.90 (d, J = 8.43 Hz, 2 H, Ph-H), 6.96–7.14 (m, 2 H, H_{ind}), 7.21 (d, J = 8.43 Hz, 2 H, Ph-H), 7.32 (d, J = 2.87 Hz, 1 H, H_{ind}), 7.46 (d, J = 7.98 Hz, 1 H, H_{ind}), 7.54 (d, J = 7.54, 1 H, H_{ind}) ppm. ^{13}C NMR (50 MHz, [D$_6$]DMSO): δ = 29.42, 29.84, 42.20, 64.57, 100.68, 109.65, 114.71, 118.94, 120.47, 121.05, 125.72, 128.12, 128.61, 130.01, 135.66, 157.70, 159.31, 159.86 ppm. IR (KBr): $\tilde{\nu}$ = 3474 (NH), 1796 (C=O), 1717 (C=N) cm^{-1}. $C_{20}H_{19}N_3O_3 \cdot {}^1/_8 H_2O$: calcd. C 68.32, H 5.48, N 11.95; found C 68.33, H 5.62, N 11.72.

3-{4-[5-(Indol-1-yl)pentoxy]benzyl}-4*H*-1,2,4-oxadiazol-5-one (III): Yellow oil, 65%. ^{1}H NMR (200 MHz, $CDCl_3$): δ = 1.4 (m, 2 H, CH_{2al}), 1.7 (m, 4 H, CH_2), 3.78 (s, 2 H, CH_2–C=N), 3.82 (t, J = 6.2 Hz, 2 H, CH_2O), 4.07 (t, J = 6.9 Hz, 2 H, CH_2N), 6.40–7.56 (m, 10 H, H_{ar}) ppm. ^{13}C NMR (50 MHz, $CDCl_3$): δ = 23.48, 28.71, 29.88, 30.59, 46.13, 67.55, 100.88, 109.22, 115.08, 119.11, 120.87, 121.26, 123.84, 127.68, 128.48, 129.85, 135.80, 158.37, 158.71, 160.95 ppm. IR (neat): $\tilde{\nu}$ = 3192 (NH), 1777 (C=O) cm^{-1}. $C_{22}H_{23}N_3O_3 \cdot {}^1/_8$ EtOAc: calcd. C 69.17, H 6.26, N 10.52; found C 69.23, H 6.40, N 10.33.

3-{4-[6-(Indol-1-yl)hexoxy]benzyl}-4*H*-1,2,4-oxadiazol-5-one (IV): Beige solid, 84%; m.p. 112.3 °C. ^{1}H NMR (200 MHz, $CDCl_3$): δ = 1.34 (m, 4 H, CH_2), 1.71 (m, 4 H, CH_2), 3.65 (s, 2 H, CH_2CN), 3.78 (t, J = 6.20 Hz, 2 H, CH_2O), 4.02 (t, J = 6.99 Hz, 2 H, CH_2N), 6.40–7.56 (m, 10 H, H_{ar}), 8.40 (br. s, 1 H, NH) ppm. ^{13}C NMR (50 MHz, $CDCl_3$): δ = 25.62, 26.62, 28.94, 30.07, 30.56, 46.15, 67.67, 100.83, 109.28, 115.05, 119.11, 120.87, 121.25, 123.84, 127.72, 128.49, 135.85, 158.60, 158.76, 161.20 ppm. IR (neat): $\tilde{\nu}$ = 3092 (NH), 1761 (C=O) cm^{-1}. $C_{23}H_{25}N_3O_3 \cdot {}^1/_2 H_2O$: calcd. C 69.00, H 6.50, N 10.50; found C 68.95, H 6.38, N 10.36.

3-{4-[7-(Indol-1-yl)heptoxy]benzyl}-4*H*-1,2,4-oxadiazol-5-one (V): Brown oil, 40%. ^{1}H NMR (200 MHz, $CDCl_3$): δ = 1.29 (m, 6 H, CH_{2al}), 1.72 (m, 4 H, CH_2), 3.70 (s, 2 H, CH_2CN), 3.81 (t, J = 6.37 Hz, 2 H, CH_2O), 4.02 (t, J = 7.03 Hz, 2 H, CH_2N), 6.40–7.56 (m, 10 H, H_{ar}), 9.90 (br. s, 1 H, NH) ppm. ^{13}C NMR (50 MHz, $CDCl_3$): δ = 25.85, 26.88, 28.92, 29.02, 30.11, 30.65, 46.30, 67.86, 100.82, 109.31, 115.15, 119.12, 120.90, 121.26, 123.77, 127.73, 128.51, 129.89, 135.88, 158.46, 158.90, 161.08 ppm. IR (neat): $\tilde{\nu}$ = 3198 (NH), 1768 (C=O) cm^{-1}. $C_{24}H_{27}N_3O_3 \cdot {}^1/_4 H_2O$: calcd. C 70.32, H 6.71, N 10.25; found C 70.58, H 6.98, N 9.92.

3-{4-[8-(Indol-1-yl)octoxy]benzyl}-4*H*-1,2,4-oxadiazol-5-one (VI): Beige solid, 52%; m.p. 86.8 °C. ^{1}H NMR (200 MHz, $CDCl_3$): δ = 1.23 (m, 8 H, CH_2), 1.68 (m, 4 H, CH_2), 3.64 (s, 2 H, CH_2CN), 3.78 (t, J = 6.41 Hz, 2 H, CH_2O), 4.00 (t, J = 7.06 Hz, 2 H, CH_2N), 6.40–7.56 (m, 10 H, H_{ar}), 9.00 (br. s, 1 H, NH) ppm. ^{13}C NMR (50 MHz, $CDCl_3$): δ = 25.84, 26.83, 29.07, 30.13, 30.56, 46.28, 67.89, 100.76, 109.30, 115.06, 119.08, 120.85, 121.21, 123.79, 127.72, 128.48, 129.88, 135.86, 158.61, 158.84, 161.19 ppm. IR (nujol): $\tilde{\nu}$ = 3098 (NH), 1765 (C=O), 1740 (C=N) cm^{-1}. $C_{25}H_{29}N_3O_3$: calcd. C 71.59, H 6.92, N 10.02; found C 71.58, H 7.14, N 9.94.

3-{4-[10-(Indol-1-yl)decoxy]benzyl}-4*H*-1,2,4-oxadiazol-5-one (VII): Brown solid, 48% yield; m.p. 74.8 °C. ^{1}H NMR (200 MHz, $CDCl_3$): δ = 1.20 (m, 12 H, CH_2), 1.69 (m, 4 H, CH_2), 3.68 (s, 2 H, CH_2CN), 3.83 (t, J = 6.37 Hz, 2 H, CH_2O), 4.02 (t, J = 7.03 Hz, 2 H, CH_2N), 6.40–7.56 (m, 10 H, H_{ar}) ppm. ^{13}C NMR (50 MHz, $CDCl_3$): δ = 25.92, 26.93, 29.15, 29.24, 29.35, 30.18, 30.62, 46.34, 68, 100.75, 109.32, 115.12, 119.08, 120.86, 121.21, 123.74, 127.74, 128.50, 129.88, 135.88, 158.51, 158.93, 161.13 ppm. IR (KBr): $\tilde{\nu}$ = 3159 (NH), 1794 (C=O), 1718 (C=N) cm^{-1}. $C_{27}H_{33}N_3O_3 \cdot {}^1/_4 H_2O$: calcd. C 71.76, H 7.41, N 9.30; found C 71.63, H 7.48, N 8.90.

Biology. Materials: Fatty-acid-free bovine serum albumin (BSA) and pancreatic PLA_2 were both purchased from Sigma (St. Louis, MO, USA). HGIIA PLA_2 was prepared as described by Dong et al.[39] The fluorescent substrate for PLA_2 assay, 1-hexadecanoyl-2-(10-pyrenedecanoyl)-*sn*-glycero-3-phosphoglycerol, ammonium salt (β-py-C_{10}-PG) was obtained from Molecular Probes (Eugene, OR, USA)-

PLA_2 Assay: The PLA_2 activity was evaluated by the method of Radvanyi et al.[40] with β-py-C_{10}-PG as substrate (2 μM final concentration). PLA_2 was used to test the potency of various inhibitors. We have shown the specificity of this assay for detecting secretory PLA_2, since the cytosolic PLA_2 was not active on substrates with a pyrene group at the *sn*-2 position.[39] In a total volume of 1 mL, the standard reaction medium contained: 50 mM Tris-HCl (pH = 7.5), 500 mM NaCl, 1 mM EGTA, 2 μM substrate, fatty-acid-free BSA solution in water (0.1%) and 6 ng mL^{-1} of pancreatic PLA_2 or 1 ng mL^{-1} of synthesized PLA_2. The fluorescence (λ_{ex} = 342 nm and λ_{em} = 398 nm) of the enzymatic reaction medium was recorded for 3 min with a spectrofluorimeter (LS 50 Perkin–Elmer) fitted with a xenon lamp. The reaction was then initiated by addition of $CaCl_2$ (10 mM, final concentration). The increase in fluorescence was continuously recorded for 1 min and the PLA_2 activity was calculated as described by Radvanyi et al.[40] When used, the inhibitor was added to the reaction medium after introduction of BSA. The activity was expressed in μmol of fluorescent β-py-C_{10}-PG hydrolyzed per min. The standard error of the mean of three independent experiments was less than 10%. This allowed the determination of the IC_{50} values (concentration of inhibitors producing 50% inhibition) of each compound.

Determination of log *P*: The partition coefficient (log *P*) of 3-(4-methoxybenzyl)-4*H*-1,2,4-oxadiazol-5-one in *n*-octanol and a phosphate buffer (40 mM, pH = 7.4) containing 15 mM NaCl was measured and the result was found to be 0.33 ± 0.04 log *P* units. The contribution of oxadiazolone was deduced from this value, by use of the hydrophobic fragmental constants system published by Rekker,[41] and we found that it represented –2.1 log *P* units. Finally, the partition coefficients (log *P*) of all described compounds were calculated with both the oxadiazolone log *P* and Rekker's hydrophobic fragmental constants.

Acknowledgments

This work was supported by grants from the CNRS and the INSERM in the French 2000–2002 national program "Molécules et Cibles Thérapeutiques". We thank the computer centers of CNRS-IDRIS, CINES Montpellier, and CCR Jussieu for their technical support. D. A. is the recipient of a grant from the CNRS, Lebanon.

[1] H. Arita, T. Nakano, K. Hanasaki, *Prog. Lipid Res.* **1989**, *28*, 273–301.
[2] G. Lambeau, M. Lazdunski, *Trends Pharmacol. Sci.* **1999**, *20*, 162–170.
[3] A. E. Denis, *J. Biol. Chem.* **1994**, *269*, 13057–13060.
[4] R. L. Heinrikson, E. T. Krueger, P. S. Keim, *J. Biol. Chem.* **1977**, *252*, 4913–4921.
[5] M. Waite, *The Phospholipases*, *in Handbook of Lipids Research*, Plenum Press, New York, **1987**, pp. 1–132.
[6] E. Valentin, R. S. Koduri, J.-C. Scimeca, G. Carle, M. H. Gelb, M. Ladunski, G. Lambeau, *J. Biol. Chem.* **1999**, *274*, 19152–19160.

[7] E. Valentin, F. Ghomaschi, M. H. Gelb, M. Ladunski, G. Lambeau, *J. Biol. Chem.* **1999**, *274*, 31195–31202.
[8] J. Ishizaki, N. Suzuki, K. Higashino, Y. Yokota, T. Ono, K. Kawamoto, N. Fujii, H. Arita, K. Hanasaki, *J. Biol. Chem.* **1999**, *274*, 24973–24979.
[9] E. Valentin, G. Lambeau, *Biochim. Biophys. Acta* **2000**, *1488*, 59–70.
[10] N. Suzuki, J. Ishizaki, Y. Yokota, K. Higashino, T. Ono, M. Ikeda, N. Fujii, H. Arita, K. Hanasaki, *J. Biol. Chem.* **2000**, *275*, 5785–5793.
[11] E. Valentin, F. Ghomashchi, M. H. Gelb, M. Lazdunski, G. Lambeau, *J. Biol. Chem.* **2000**, *275*, 7492–7496.
[12] M. H. Gelb, E. Valentin, F. Ghomashchi, M. Lazdunski, G. Lambeau, *J. Biol. Chem.* **2000**, *275*, 39823–39826.
[13] J. D. Clark, N. Milona, J. L. Knopf, *Proc. Natl. Acad. Sci. USA* **1990**, *87*, 7708–7712.
[14] J. D. Clark, L.-L. Lin, R. W. Kriz, C. S. Ramesha, L. A. Sultzman, A. Y. Lin, N. Milona, J. L. Knopf, *Cell* **1991**, *65*, 1043–1051.
[15] H. Van Den Bosch, A. J. Aarsman, H. M. Verkleij, *New Trends in Lipid Mediators Research*, Karger Editions, Basel, **1989**, pp. 257–261.
[16] M. D. Rosenthal, M. N. Gordon, E. S. Buescher, J. H. Slusser, L. K. Harris, R. C. Franson, *Biochem. Biophys. Res. Commun.* **1995**, *208*, 650–656.
[17] A. J. Aarsman, J. G. N. De Jong, E. Arnoldussen, F. W. Neys, P. D. Van Wassenaar, H. Van Den Bosch, *J. Biol. Chem.* **1989**, *264*, 10008–10014.
[18] T. Minami, H. Tojo, Y. Shinomura, Y. Matsusawa, M. Okamoto, *Biochim. Biophys. Acta* **1993**, *1170*, 125–130.
[19] R. D. Dillard, N. J. Bach, S. E. Draheim, D. R. Berry, D. G. Carlson, N. Y. Chirgadze, D. K. Clawson, L. W. Hartley, L. M. Johnson, N. D. Jones, E. M. McKinney, E. D. Mihelich, J. L. Olkowski, R. W. Schevitz, A. C. Smith, D. W. Snyder, C. D. Sommers, J. P. Wery, *J. Med. Chem.* **1996**, *39*, 5137–5158.
[20] R. D. Dillard, N. J. Bach, S. E. Draheim, D. R. Berry, D. G. Carlson, N. Y. Chirgadze, D. K. Clawson, L. W. Hartley, L. M. Johnson, N. D. Jones, E. M. McKinney, E. D. Mihelich, J. L. Olkowski, R. W. Schevitz, A. C. Smith, D. W. Snyder, C. D. Sommers, J. P. Wery, *J. Med. Chem.* **1996**, *39*, 5119–5136.
[21] S. E. Draheim, N. J. Bach, R. D. Dillard, D. R. Berry, D. G. Carlson, N. Y. Chirgadze, D. K. Clawson, L. W. Hartley, L. M. Johnson, N. D. Jones, E. M. McKinney, E. D. Mihelich, J. L. Olkowski, R. W. Schevitz, A. C. Smith, D. W. Snyder, C. D. Sommers, J. P. Wery, *J. Med. Chem.* **1996**, *39*, 5139–5175.
[22] P. C. Unangst, G. P. Shrum, D. T. Connor, R. D. Dyer, D. J. Schrier, *J. Med. Chem.* **1992**, *35*, 3691–3968.
[23] S.-S. Cha, D. Lee, J. Adams, J. T. Kurdyla, C. S. Jones, L. A. Marshall, B. Bolognese, S. S. Abdel-Meguid, B.-H. Oh, *J. Med. Chem.* **1996**, *39*, 3878–3881.
[24] M. Aïdafoun, C. Mounier, F. Heymans, C. Binisti, C. Bon, J.-J. Godfroid, *Biochem. Pharmacol.* **1996**, *51*, 737–742.
[25] J. Ma, D. Dougherty, *Chem. Rev.* **1997**, *97*, 1303–1324.
[26] W. Dehaen, A. Hassner, *J. Org. Chem.* **1991**, *56*, 896–900.
[27] F. Heymans, L. Assogba, C. Z. Dong, J.-J. Godfroid, French Patent, No. 9906366, **1999**.
[28] H. Van de Waterbeemd, D. A. Smith, K. Beaumont, D. K. Walker, *J. Med. Chem.* **2001**, *44*, 1313–1333.
[29] N. Gresh, *J. Comput. Chem.* **1995**, *16*, 856.
[30] J. Langlet, P. Claverie, J. Caillet, A. Pullman, *J. Phys. Chem.* **1988**, *92*, 1631–1643.
[31] J. Antony, N. Gresh, L. Hemmingsen, L. Olsen, C. Schofield, R. Bauer, *J. Comput. Chem.* **2002**, *23*, 1281–1296.
[32] N. Gresh, B. P. Roques, *Biopolymers* **1997**, *47*, 145–164.
[33] B. Roux, T. Simonson, *Biophys. Chem.* **1999**, *78*, 1–20.
[34] T. Simonson, *Curr. Opin. Struct. Biol.* **2001**, *11*, 243–252.
[35] Accelrys Inc., 9685 Scranton Rd., San Diego, CA 92121-3752, USA.
[36] M. J. Frisch, A. Frisch, in *Gaussian 98*, *User's Reference*, Gaussian, Inc., Pittsburg, PA, **1999**, and references therein.
[37] W.-Q. Liu, M. Vidal, N. Gresh, B. P. Roques, C. Garbay, *J. Med. Chem.* **1999**, *42*, 3737–3741.
[38] B. Honig, K. Sharp, A.-S. Yang, *J. Phys. Chem.* **1993**, *97*, 1101–1109.
[39] C. Z. Dong, A. Romieu, C. M. Mounier, F. Heymans, B. P. Roques, J.-J. Godfroid, *Biochem. J.* **2002**, *365*, 505–511.
[40] F. Radvanyi, L. Jordan, F. Russo-Marie, C. Bon, *Anal. Biochem.* **1989**, *177*, 103–109.
[41] R. F. Rekker, H. M. De Koort, *Eur. J. Med. Chem. Chim. Ther.* **1979**, *14*, 479–488.

Received: July 30, 2004

